Chapter

Controllable Synthesis of Few-Layer Graphene on β-SiC(001)

Olga V. Molodtsova, Alexander N. Chaika and Victor Yu. Aristov

Abstract

Few-layer graphene exhibits exceptional properties that are of interest for fundamental research and technological applications. Nanostructured graphene with self-aligned domain boundaries and ripples is one of very promising materials because the boundaries can reflect electrons in a wide range of energies and host spin-polarized electronic states. In this chapter, we discuss the ultra-high vacuum synthesis of few-layer graphene on the technologically relevant semiconducting β-SiC/Si(001) wafers. Recent experimental results demonstrate the possibility of controlling the preferential domain boundary direction and the number of graphene layers in the few-layer graphene synthesized on the β-SiC/Si(001) substrates. Both these goals can be achieved utilizing vicinal silicon wafers with small miscuts from the (001) plane. This development may lead to fabricating new tunable electronic nanostructures made from graphene on β-SiC, opening up opportunities for new applications.

Keywords: silicon carbide, graphene, synthesis, nanodomains, ARPES, LEEM, μ-LEED, XPS, STM

1. Introduction

Extensive studies of mono- and few-layer graphene films, conducted during the last two decades, have revealed unique electronic properties of these low-dimensional materials [1–7], which make them very promising for developing new nanoscale carbon-based electronic technologies [8–13]. Its unique transport properties make graphene a very attractive alternative to silicon in the traditional electronic technologies. However, for successful applications, it is necessary to develop methods of synthesizing low-cost, high-quality graphene films on insulating or semiconducting substrates of sufficiently large size.

Many methods of fabricating ultrathin graphene films have been reported. For example, graphene can be prepared using mechanical or chemical exfoliation from bulk graphite crystals [1, 3, 4, 14]. The mechanically exfoliated graphene layers demonstrate exceptional properties of two-dimensional electron gas, such as extremely high mobility of the charge carriers [15, 16]. However, the exfoliated graphene layers are hardly suitable for technological purposes. The procedures using unzipping of carbon nanotubes, reduction of graphite oxide, chemical vapor deposition, and high-temperature thermal graphitization of single-crystalline substrates were developed to fabricate large-area graphene films [1, 17–22]. To eliminate possible problems associated with the graphene film transfer from one

substrate to another, various methods have been developed for direct growing graphene on the technologically relevant non-conducting substrates [23–30].

The hexagonal silicon carbide (α-SiC) wafers are considered the most promising semiconducting substrates for technological synthesis of high-quality graphene films [31–37]. Ultrathin graphene films are usually fabricated on α-SiC using silicon atom sublimation and graphitization of the carbon-enriched surface layers at temperatures above 1000°C [31]. Epitaxial graphene layers synthesized on α-SiC in ultra-high vacuum (UHV) and argon atmosphere demonstrate 2D electronic properties [38–41], which are nearly equivalent to the properties of ultrathin graphene films mechanically exfoliated from bulk graphite crystals. The angle resolved photoelectron spectroscopy (ARPES) studies of the 11-layer graphene on 6H-SiC(000-1) revealed sharp linear dispersions at the K-points typical of monolayer graphene [42].

However, the high price and small size of the single-crystalline α-SiC wafers are not compatible with commercial applications. In order to reduce the price of SiC wafers, epitaxial growth of cubic silicon carbide (β-SiC) thin films on silicon wafers was proposed in the 1980s [43]. Using this method, β-SiC thin films with thickness of several microns could be grown on standard silicon wafers with diameters above 30 cm [44–47] that is highly appealing for direct integration into existing electronic technologies. Fabrication of ultrathin graphene films on β-SiC surfaces, using high-temperature annealing in UHV, was reported for the first time in 2009, when Miyamoto et al. succeeded in synthesizing few-layer graphene on the β-SiC/Si(011) wafers [48]. Then, a number of works demonstrating the feasibility of graphene synthesis on β-SiC/Si wafers of different orientations have been published [48–103]. Mostly, these studies have been conducted on β-SiC(111) thin films [51–61, 65–81] and single-crystalline SiC(111) wafers [62–64]. However, some studies have been carried out on β-SiC(001) [50, 61, 82–93, 101, 102] and even on polycrystalline β-SiC substrates [94]. Since Si(001) is widely used in electronic devices, few-layer graphene films synthesized on the β-SiC/Si(001) wafers can be fully compatible with the existing lithographic processing technologies.

This chapter is focused on the controllable UHV synthesis of few-layer graphene on the β-SiC thin films grown on the technologically relevant Si(001) wafers. Along with detailed atomic and electronic structure studies we present the recent results which uncover the mechanism of layer-by-layer graphene growth on β-SiC/Si(001) and pave the way to synthesize uniform few-layer graphene nanoribbons with desirable number of layers and self-aligned nanodomain boundaries on the low-cost silicon wafers.

2. Atomic and electronic structure of few-layer graphene synthesized on β-SiC/Si(001)

Few-layer graphene synthesis on the β-SiC/Si(001) wafers was demonstrated for the first time in the near-edge X-ray absorption fine structure (NEXAFS), core-level photoelectron spectroscopy (PES), ARPES, and local scanning tunneling microscopy (STM) experiments [50]. Later, the few-layer graphene formation on the β-SiC/Si(001) substrates during high-temperature annealing in UHV was proved by independent Raman spectroscopy experiments [82]. These works showed quasi-free-standing character of the synthesized graphene overlayers. Raman spectroscopy data also revealed the presence of a large number of defects in the few-layer graphene grown on the β-SiC/Si(001) wafers with the average distance between them on the order of 10 nm [82]. However, the origin of these defects could be uncovered only in comprehensive studies using a set of complementary

high-resolution micro-spectroscopic techniques, namely, low energy electron microscopy (LEEM), micro low energy electron diffraction (μ-LEED), core-level PES, ARPES, and atomic-resolution STM [85, 87].

Figure 1 shows typical large-area STM images taken from a β-SiC(001) surface before and after trilayer graphene synthesis in UHV [85, 87]. The image of the β-SiC(001)-c(2 × 2) structure (**Figure 1(a)**) reveals extra carbon atoms (bright protrusions) on the surface and monatomic steps. The root mean square (RMS) roughness analysis of the STM images demonstrates substantial enhancement of the surface roughness after the trilayer graphene synthesis. For comparison, the histograms calculated from the STM images of the same size (100 × 100 nm^2) before and after trilayer graphene synthesis are shown on **Figure 1(d)**, **(i)**, and **(j)**. Note that RMS of

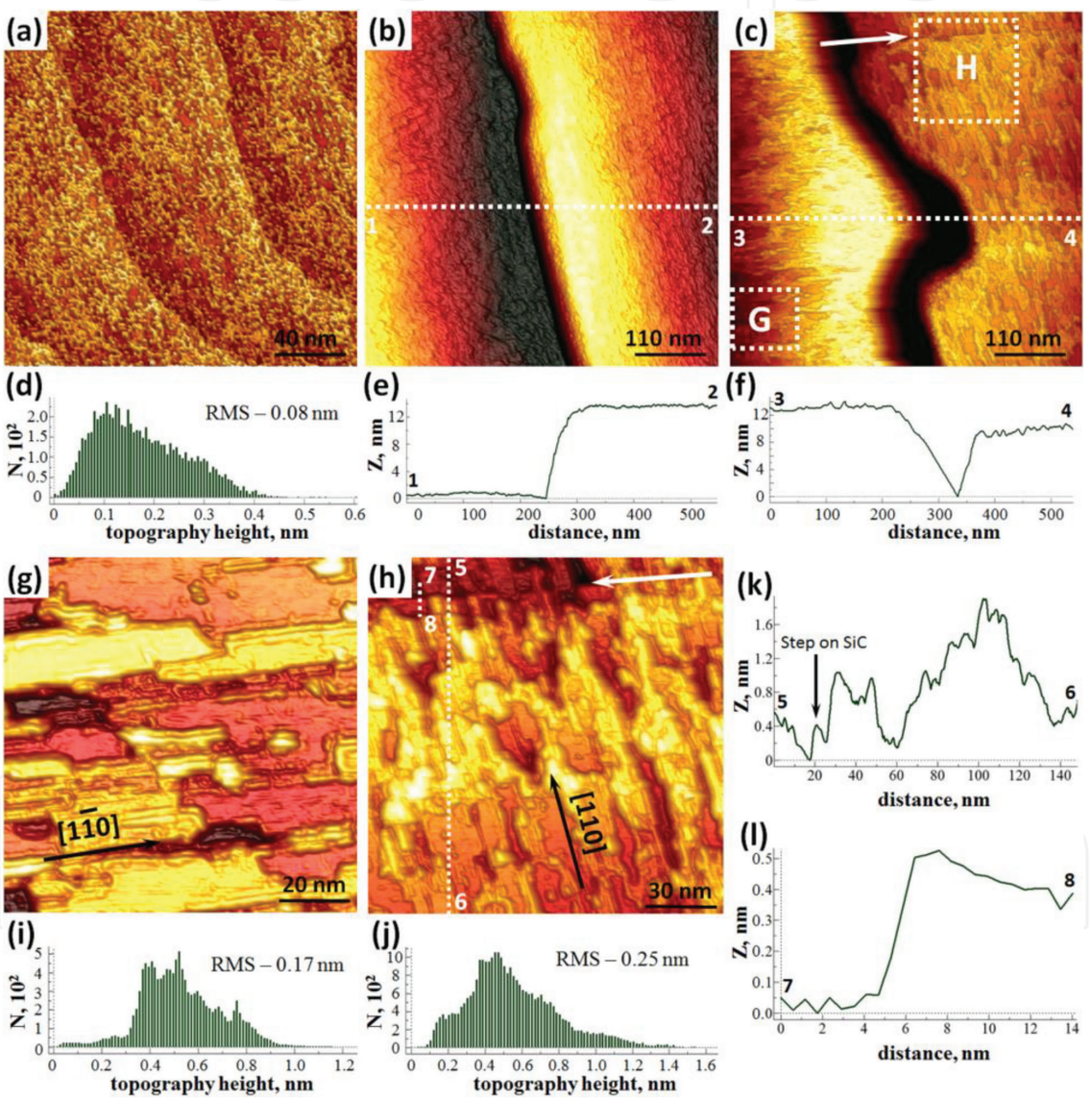

Figure 1.
Large-area STM images of SiC(001)-c(2 × 2) (a) and trilayer graphene/SiC(001) ((b), (c), (g), and (h)). Panels (b) and (c) illustrate the continuity of the graphene overlayer near the multiatomic step (b) and APD boundary (c). The images in panels (g) and (h) emphasize the nanodomains elongated along the [1$\bar{1}$0] (g) and [110] directions (h) observed on the left (area G) and right side (area H) of the APD boundary in panel (c), respectively. The STM images were measured at U = −3.0 V and I = 60 pA (a), U = −1.0 V and I = 60 pA (b), U = −0.8 V and I = 50 pA (c), U = −0.8 V and I = 60 pA (g), and U = −0.7 V and I = 70 pA (h). The white arrows in panels (c) and (h) indicate a monatomic step on the SiC substrate. (d), (i), and (j) Roughness analysis of the STM images in panels (a), (g), and (h). The histograms were calculated from surface areas of the same size (100 × 100 nm^2) for direct comparison of the surface roughness before and after trilayer graphene synthesis. (e), (f), (k), and (l) Cross-sections (1–2), (3–4), (5–6), and (7–8) of the images in panels (b), (c), and (h). Reproduced from Ref. [87] with permission of IOP.

micrometer-scale β-SiC(001)-c(2 × 2) STM images typically varied between 1.0 and 1.5 Å, while the RMS values calculated from the images of trilayer graphene were in the range of 3.0–5.0 Å. The increase of the surface roughness after graphene synthesis is related to the atomic-scale rippling typical for free-standing graphene [104, 105]. STM investigations conducted in different surface areas of several samples [87] confirmed the continuity of the few-layer graphene films covering the β-SiC/Si(001) wafers. As an example, **Figure 1(b)** and **(c)** shows STM images measured at bias voltages corresponding to the bandgap of β-SiC. STM imaging was stable even in the vicinity of multiatomic steps (**Figure 1(b)**) and anti-phase domain (APD) boundaries (**Figure 1(c)**), separating the areas where the β-SiC crystal lattice is rotated by 90°.

STM studies [85, 87] showed that the top graphene layer consists of nanodomains connected to one another through domain boundaries (**Figure 1(g)** and **(h)**). The nanodomain boundaries (NBs) are preferentially aligned with the two orthogonal <110> directions of the SiC crystal lattice, as indicated in **Figure 1(g)** and **(h)**. The domains are elongated in the [110] and [1$\bar{1}$0] directions on the right and left side of the APD boundary, respectively (**Figure 1(c)**). The length and width of the nanodomains on the SiC(001) substrate were in the range of 20–200 nm and 5–30 nm, respectively. These values correlate well with the average distance between defects derived from the Raman spectroscopy studies [82].

The continuity and uniform thickness of the graphene overlayer synthesized on the β-SiC/Si(001) wafers were confirmed in the LEEM experiments (**Figure 2**). The bright-field (BF) LEEM image measured at small electron energy shows uniform contrast throughout the all probed micrometer-sized surface area, including the regions containing defects (steps and APD boundaries). The number of graphene layers can be determined from the number of oscillations in the reflectivity *I-V* curves measured in a small energy window [106, 107]. In the reflectivity spectra shown on **Figure 2(h)**, one can see three reproducible minima, which correspond to the uniform trilayer graphene coverage. The graphene film thickness is homogeneous

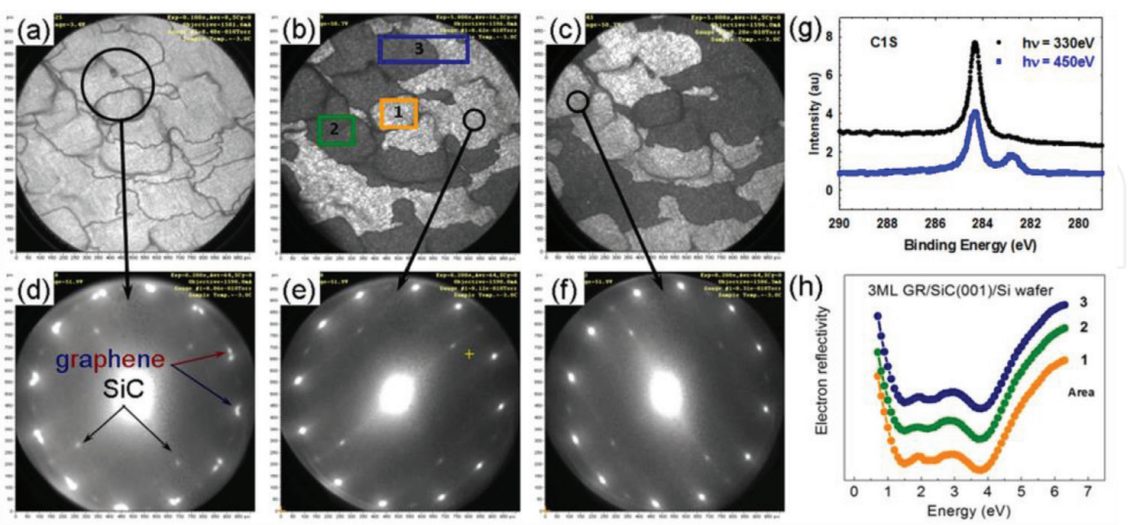

Figure 2.
(a) 20 μm BF LEEM micrograph, recorded with an electron energy of 3.4 eV, proving the uniform thickness of trilayer graphene on β-SiC/Si(001) wafers. (b) and (c) DF LEEM images from different diffraction spots (shown in panels (e) and (f)) demonstrating the contrast reversal on micrometer-scale areas with two rotated graphene domain families. (d)–(f) μ-LEED patterns from the surface areas shown by black circles in panels (a)–(c). The diameters of the sampling areas are 5 μm (a) and 1.5 μm ((b) and (c)), E = 52 eV. (g) μ-PES C 1s spectra taken at two photon energies. The diameter of the probed area is 10 μm. (h) Electron reflectivity spectra recorded for surface regions 1, 2, and 3 as labeled in panel (b). Reproduced from [85] with permission of Tsinghua and Springer.

over the surface and *I-V* curves are almost identical in the surface areas appearing dark and white in the dark-field (DF) LEEM images, as **Figure 2(h)** illustrates.

The μ-LEED patterns taken from micrometer-sized surface areas (**Figure 2(d)**) typically revealed 12 sharp double-split spots and 12 substantially less intense singular spots, corresponding to the nanostructured graphene, and singular spots from the SiC(001) substrate. The μ-LEED patterns measured from different APDs (**Figure 2(e)** and **(f)**) demonstrate 12 non-equidistant spots and six less intense singular graphene spots. The diffraction patterns measured from the APDs are rotated relative to one another by 90°. These LEEM and μ-LEED data demonstrate that each micrometer-sized APD contains graphene nanodomain families with three preferential lattice orientations, giving six preferential lattice orientations on larger (millimeter-scale) surface areas. For the trilayer graphene, four of these six lattice orientations are prevailing in the top layer. The core-level C 1*s* spectra measured from this sample (**Figure 2(g)**) demonstrate only two components with binding energies (BE) corresponding to silicon carbide (lower BE) and graphene (higher BE) in accordance with other core-level PES studies [50], proving the weak interaction of the few-layer graphene with β-SiC(001).

Atomically resolved STM studies presented in **Figure 3** disclose the origin of 12 double-split spots in the LEED patterns (**Figure 2(d)**). STM images in **Figure 3(a)** and **(b)** demonstrate nanodomains elongated in the [110] and [1$\bar{1}$0] directions, respectively. The 2D fast Fourier transform (FFT) of the STM images consists of two systems of spots, which are related to two graphene lattices rotated by 27°. Inset in **Figure 3(b)** shows one of the FFT patterns. According to the μ-LEED data (**Figure 2(e)** and **(f)**), the graphene domain lattices are

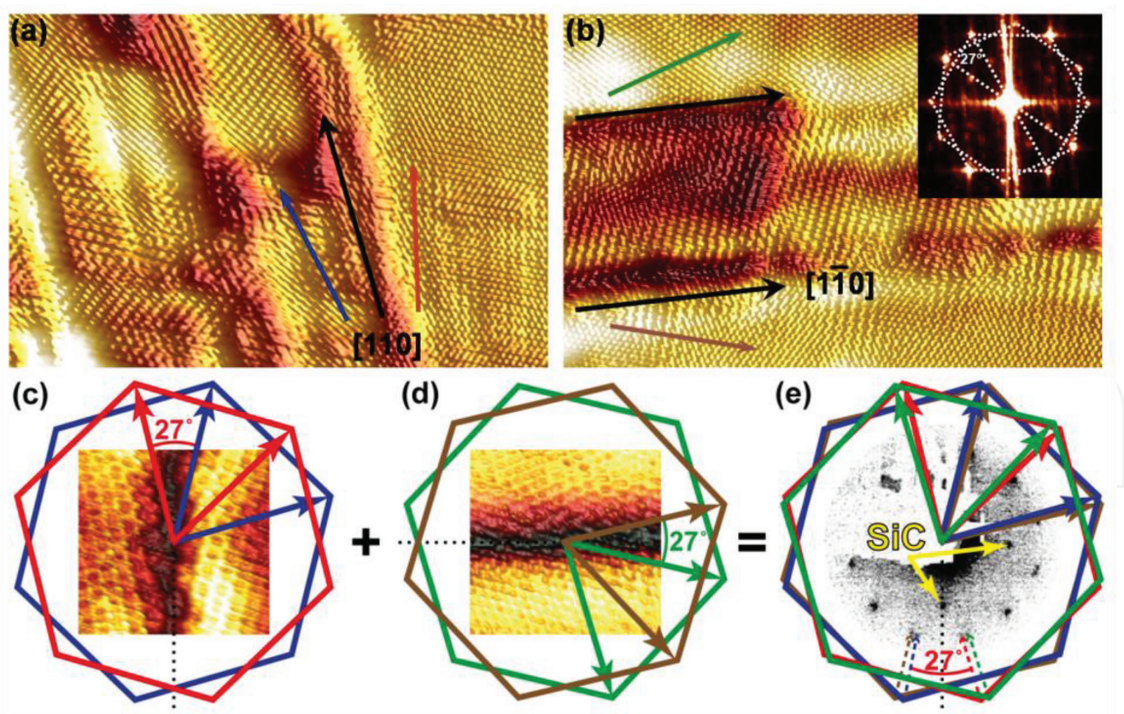

Figure 3.
(a and b) 19.5 × 13 nm² atomically resolved STM images of trilayer graphene nanodomains on SiC(001) elongated along the [110] (a) and [1$\bar{1}$0] directions (b). The images were taken from different surface areas at U = −10 mV and I = 60 pA. The inset in panel (b) shows an FFT pattern with two 27°-rotated systems of spots. (c–e) Models explaining the origin of the 12 double-split diffraction spots in the LEED pattern shown in Figure 2(d). The insets in panels (c) and (d) are STM images of the <110>-directed domain boundaries. The four differently colored hexagons—red, blue, green, and brown—represent the four preferential domain lattice orientations. The inset in panel (e) shows a LEED pattern taken at E_p = 65 eV, demonstrating 1 × 1 substrate spots (highlighted by yellow arrows) along with 12 double-split graphene spots, indicated by one dotted arrow for each orientation. Reproduced from Ref. [87] with permission of IOP.

preferentially rotated by ±13.5° from the [110] and [1$\bar{1}$0] crystallographic directions of the substrate, which almost coincide with the preferential directions of the nanodomain boundaries. These two families of 27°-rotated domains are rotated by 90° relative to one another and produce two systems of 12 non-equidistant spots in the FFT and μ-LEED patterns (e.g. see **Figure 2(e)** and **(f)**). The sum of two 90°-rotated patterns with 12 non-equidistant spots produce the LEED pattern of graphene/β-SiC/Si(001) with 12 double-split spots, as the models shown in **Figure 3(c–e)** illustrate. These two orthogonal 27°-rotated domain families are usually resolved as horizontal and vertical nanoribbons in STM experiments (**Figure 1(g)** and **(h)**). The DF LEEM images taken from different reflexes in either of the double-split spots show a reversed contrast and confirm that the 27°-rotated domain families typically cover micrometer-sized surface regions in different APDs (**Figure 2(b)** and **(c)**).

Atomic-resolution STM images of the trilayer graphene on β-SiC(001) measured inside the nanodomains usually revealed either hexagonal (**Figure 4(a)**) or honeycomb (**Figure 4(d)**) patterns distorted by atomic-scale rippling [104]. The line profile shown in **Figure 4(c)** reveals random vertical corrugations related to the atomic-scale rippling and regular oscillations with a period of ~ 2.5 Å corresponding to the graphene honeycomb lattice. Typical dimensions of the ripples are about several nanometers laterally and 1 Å vertically (**Figure 4(b)**), coinciding with values predicted by the theory for free-standing monolayer graphene [104]. The random picometer-scale distortions of the sp^2-hybridized carbon bond lengths in graphene/β-SiC/Si(001) are illustrated using smaller area STM images presented in **Figure 4(d–f)**.

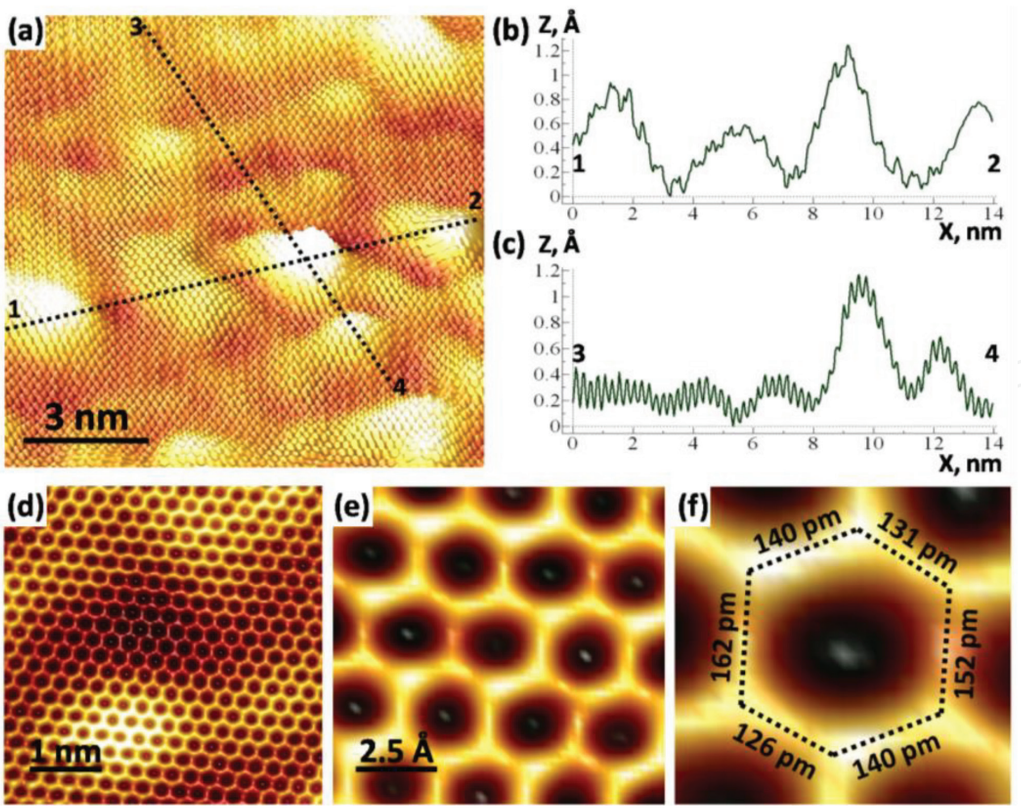

Figure 4.
(a) 13.4 × 13.4 nm² STM image of trilayer graphene on β-SiC(001), illustrating atomic-scale rippling. The image was measured at U = 0.1 V and I = 60 pA. (b) and (c) Cross-sections (1–2) and (3–4) from the image in panel (a). (d–f) STM images of the trilayer graphene, demonstrating random picometer-scale distortions of the honeycomb lattice. The images were measured at U = 22 mV and I = 70 pA (d) and U = 22 mV and I = 65 pA (e and f). One of the distorted hexagons is shown in (f) for clarity. Reproduced from Ref. [103] with permission of Elsevier.

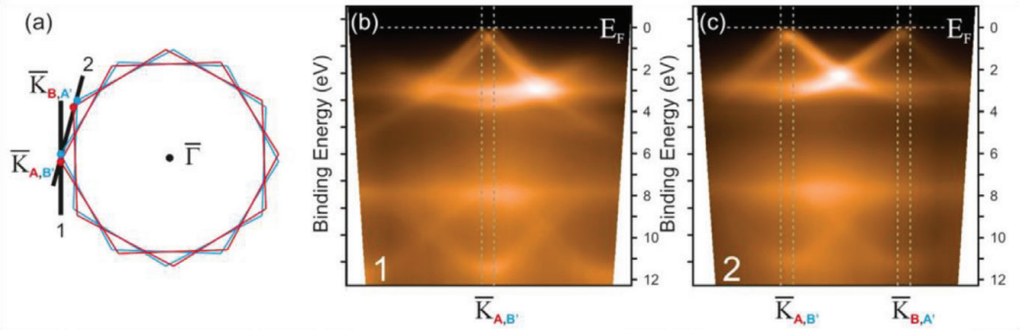

Figure 5.
ARPES characterization of trilayer graphene grown on β-SiC(001). (a) Effective surface Brillouin zone due to superposition of four rotated domain variants (A, B, A', and B'). (b) and (c) Dispersion of π-band in graphene measured along directions 1 and 2 in (a). Reproduced from Ref. [85] with permission of Tsinghua and Springer.

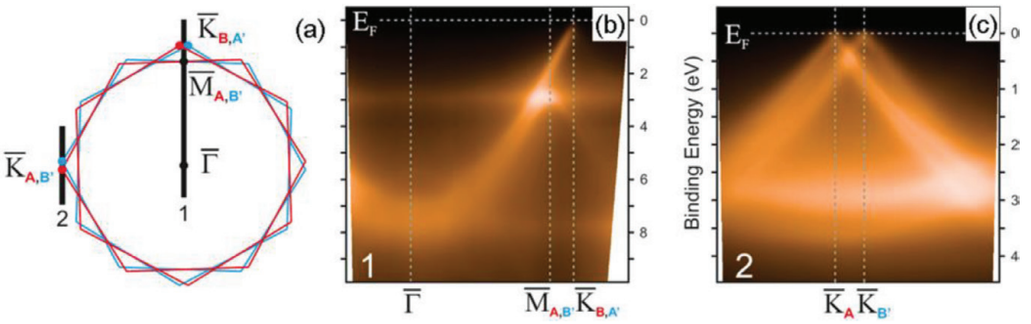

Figure 6.
ARPES characterization of trilayer graphene grown on β-SiC(001). (a) Effective surface Brillouin zone due to superposition of four domain lattices (A, B, A', and B'). (b) and (c) Dispersion of π-band in trilayer graphene measured by ARPES along directions 1 and 2 in (a). Reproduced from Ref. [85] with permission of Tsinghua and Springer.

The uniformity of the atomic and electronic structure of the trilayer graphene/β-SiC/Si(001) on a millimeter-scale was confirmed by ARPES [85]. As an example, the photoemission studies of the π band are shown in **Figures 5** and **6**. Since ARPES technique probes millimeter-scale sample areas, the effective surface Brillouin zone of graphene on β-SiC(001) comprises Brillouin zones of all rotated lattices (**Figure 5(a)**). The identical sharp linear dispersions typical of quasi-free-standing graphene are observed for all rotated domain variants (**Figure 5(b)** and **(c)**), with the Dirac points located at the Fermi level. The ARPES dispersion measured from the trilayer graphene/β-SiC/Si(001) sample along the $\overline{\Gamma} - \overline{K}$-direction of the surface Brillouin zone (**Figure 6(b)**) reveals the π band reaching the Fermi level. **Figure 6(b)** also displays a dispersion of the π band that backfolds at ~2.5 eV BE and originates from the *M*-point of the rotated graphene domain. In order to determine the position of the Dirac point, the dispersions were measured in a detection geometry perpendicular to the $\overline{\Gamma} - \overline{K}$-direction (short black line in **Figure 6(a)**) where the interference effects are suppressed and both sides of the Dirac cone are observed [108]. The ARPES data shown in **Figure 6(c)** reveal sharp linear dispersions and tiny additional bands between the two split Dirac cones. According to the theoretical calculations presented in Ref. [93], the observed ARPES dispersions may correspond to a quasi-free-standing Bernal-stacked ABA-trilayer graphene formed on β-SiC(001).

The experimental data presented in this section were obtained during high-resolution studies of the trilayer graphene grown on a low-index β-SiC/Si(001) wafer using high-temperature annealing in UHV. They demonstrate the fabrication of uniform nanostructured graphene with two preferential NB directions

on millimeter-sized samples. Such nanoribbon systems supported on the Si(001) wafers are very promising because the presence of the self-aligned boundaries can provide a sizeable energy gap in graphene [10]. However, for technological applications it is highly desirable to control the thickness of the graphene overlayer and reduce the number of the preferential NB orientations from two to one. Note that thickness of the few-layer graphene synthesized on β-SiC/Si(001) wafers by different groups, utilizing very similar UHV thermal treatment procedures, varied from one to several monolayers [50, 82–93, 101].

3. Layer-by-layer graphene growth on β-SiC/Si(001)

For detailed understanding the mechanisms of the surface transformation and layer-by-layer graphene growth on β-SiC/Si(001) in UHV at high temperatures a series of experimental studies with *in-situ* control of the surface atomic and electronic structure during heating have been conducted [102, 109]. **Figure 7** summarizes the β-SiC(001) surface transformations during annealing in UHV, monitored using *in-situ* core-level PES (**Figure 7(a–g)**) and *ex-situ* LEED and STM (**Figure 7(h–l)**).

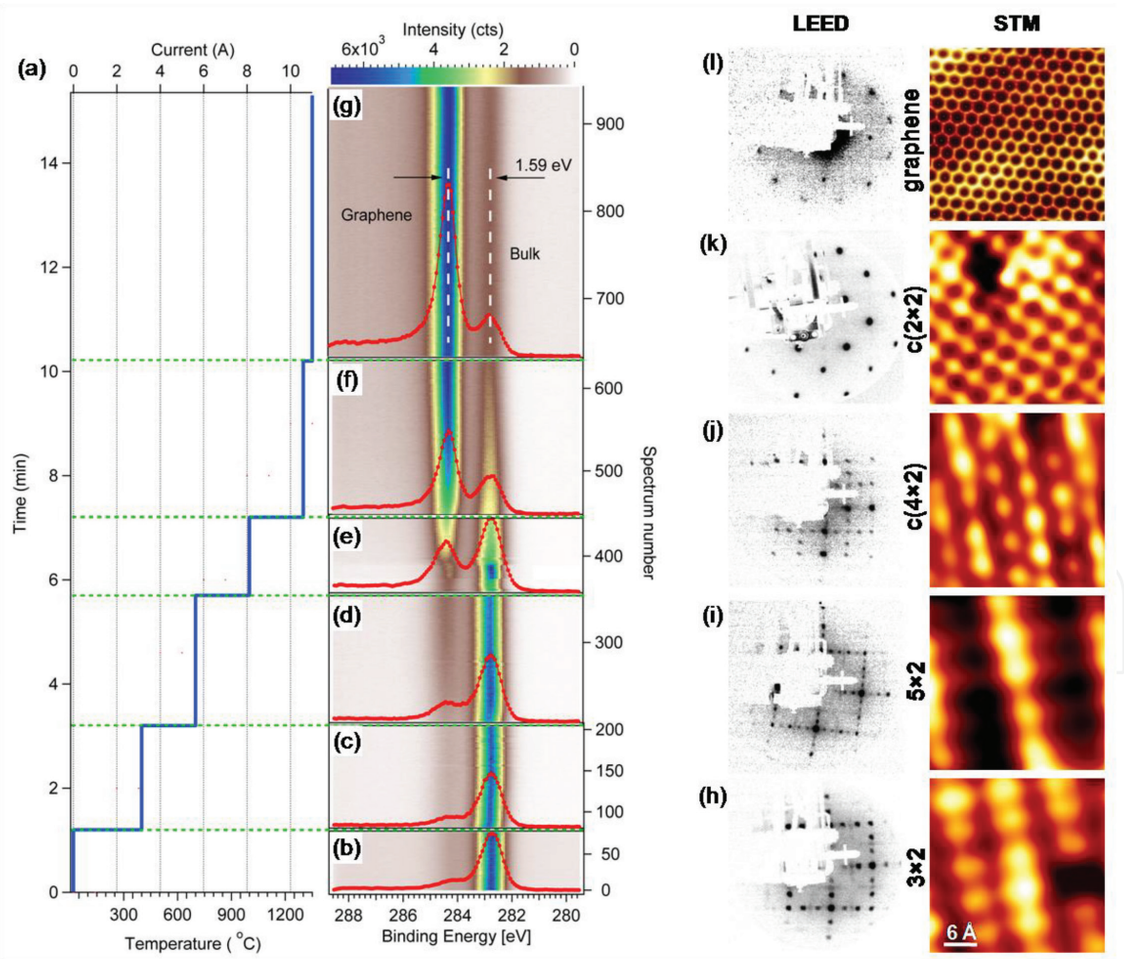

Figure 7.
(a–g) In-situ core-level PES studies of β-SiC/Si(001) during heating in UHV. (a) Temperature of the sample during the PES measurements. (b–g) Time evolution of the C 1s core-level spectra recorded in snapshot regime during heating. A single spectrum taken in the corresponding temperature interval (shown in panel (a)) is presented. (h–l) Evolution of the SiC(001) surface atomic structure probed by LEED and STM. The 3 × 2, 5 × 2, c(4 × 2), and c(2 × 2) reconstructions are consecutively formed on the SiC(001) surface in the temperature range of 800–1300°C before the graphene overlayer formation. Reproduced from Ref. [109] with permission of Elsevier.

The first steps toward successful graphene synthesis on β-SiC/Si(001) relate to the removal of the protective silicon oxide layer and the fabrication of a contaminant-free SiC(001)1 × 1 surface structure. This reconstruction can be fabricated after outgassing the sample holder and flash-heating the β-SiC/Si(001) wafers at 1000–1100°C. Then, the fabrication of a graphene overlayer includes the deposition of several monolayers (MLs) of silicon atoms onto the clean, carbon-rich SiC(001)1 × 1 surface and annealing at gradually increasing temperatures. Depending on the quality of the β-SiC thin film grown on the Si(001) wafer, the deposition and annealing cycles can be repeated until sharp 1 × 1 LEED pattern is observed.

Figure 7(a–g) shows the results of the PES experiments with real-time control during the direct-current sample heating with silicon deposited onto SiC(001)1 × 1 surface structure [109]. During the measurements, a current was applied to heat the sample up to 1350°C (**Figure 7(a)**). The C 1*s* core-level spectra were taken in a snapshot mode during the sample heating with an acquisition time of 1s/spectrum, using a photon energy of 750 eV. Six core-level spectra taken at different stages of the surface graphitization are shown in **Figure 7(b–g)**. Two main C 1*s* peak components can be distinguished in the spectra, which change their relative intensity with increasing temperature. Note that the absolute (but not the relative) binding energies of the individual components in this experiment could be modified by the voltage applied across the β-SiC/Si(001) wafer.

At lower temperatures (**Figure 7(b)**), a strong peak corresponding to the bulk carbon atoms dominates in the PES spectra. At temperatures above 1200°C (**Figure 7(d–f)**), an additional component (shifted to higher BE) starts to grow, while the relative intensity of the bulk component decreases. The change of the C 1*s* core-level shape corresponds to the carbonization of the top surface layers at high temperatures. At temperatures close to the silicon melting point (1350°C), the carbon-carbon bonds undergo a transition to sp^2 hybridization corresponding to graphene lattice formation (**Figure 7(g)**). *Ex-situ* LEED measurements proved the existence of a graphene overlayer on the β-SiC/Si(001) wafer used for the PES experiments presented in **Figure 7(b–g)**.

Figure 7(h–l) shows step-by-step LEED and STM studies of the β-SiC(001) surface atomic structure after heating in UHV at various temperatures. They prove consecutive fabrication of different β-SiC(001) surface reconstructions in accordance with Refs. [110, 111]. The LEED and STM data in **Figure 7(h–l)** were obtained after consecutive heating of the same β-SiC/Si(001) sample in UHV to 1000, 1150, 1200, 1250, and 1350°C, and cooling to room temperature. After annealing at temperatures of 700–1000°C a uniform, Si-rich SiC(001)3 × 2-reconstructed surface with large (001)-oriented terraces is fabricated (**Figure 7(h)**). Increasing the annealing temperature from 1000 to 1250°C leads to consecutive fabrication of the silicon-terminated 5 × 2 (**Figure 7(i)**), c(4 × 2) (**Figure 7(j)**), 2 × 1, and carbon-terminated c(2 × 2) reconstructions (**Figure 7(k)**). According to the LEED and STM studies, the most uniform graphene overlayers on β-SiC(001) can be obtained after flash heating (10–20 s) of the c(2 × 2) reconstruction at 1350°C with post-annealing at 600–700°C, which is similar to the method used for the synthesis of graphene on α-SiC [39, 112, 113]. The LEED pattern shown in **Figure 7(l)** reveals sharp substrate spots and 12 double-split graphene spots related to the formation of the few-layer graphene nanodomain network similar to the one presented in **Figures 1** and **3**.

The exact number of the graphene layers synthesized on β-SiC(001) during UHV heating could strongly depend on the vacuum conditions, annealing temperature and duration [70]. To uncover the mechanism of the layer-by-layer graphene growth on the β-SiC/Si(001) substrates and find the way to control the number of synthesized graphene layers and preferential nanodomain boundary direction,

in-situ high-resolution core-level and angle-resolved photoelectron spectroscopy, LEEM and μ-LEED studies have been carried out [102].

Figure 8 shows μ-LEED, LEEM *I-V*, ARPES and micro X-ray photoelectron spectroscopy (μ-XPS) data obtained from the same sample region *in-situ* during the high-temperature surface graphitization in UHV. The μ-LEED pattern and C 1s core level spectra taken in bulk- and surface-sensitive regimes from the β-SiC(001)-c(2 × 2) reconstruction prepared prior to graphene synthesis are shown in **Figure 8(a)**. Then, the temperature of the β-SiC/Si(001) wafer was increased and graphene spots were observed in the μ-LEED patterns. The first graphene monolayer (**Figure 8(b)**) was formed after 10 short flashes at temperatures in the range from 1250 to 1300°C and pressures not exceeding 5×10^{-9} mbar. For the fabrication of 2 and 3 ML graphene (**Figure 8(c)** and **(d)**), 50 and 100 flash heating cycles, respectively, were applied at 1300°C. The number of the synthesized graphene layers was defined from the number of minima in the low energy part of the electron reflectivity *I-V* curves presented in **Figure 8** (top). The graphs in **Figure 8** (bottom) depict the evolution of the C 1s spectra acquired in normal emission from a circular sample area (d = 2 μm) at 325, 330, 400, and 450 eV photon energies for a SiC(001)-c(2 × 2) reconstruction **(a)**, mono- **(b)**, bi- **(c)**, and trilayer graphene **(d)**. The selected photon energies correspond to different surface sensitivities of the XPS measurements with the highest sensitivity achieved at 325 and 330 eV. The C 1s spectra were decomposed into individual components corresponding to different carbon atom chemical bonds [102]. The results of the C 1s spectra decomposition are presented in **Figure 8** together with the experimental data (black circles) where the red line is the

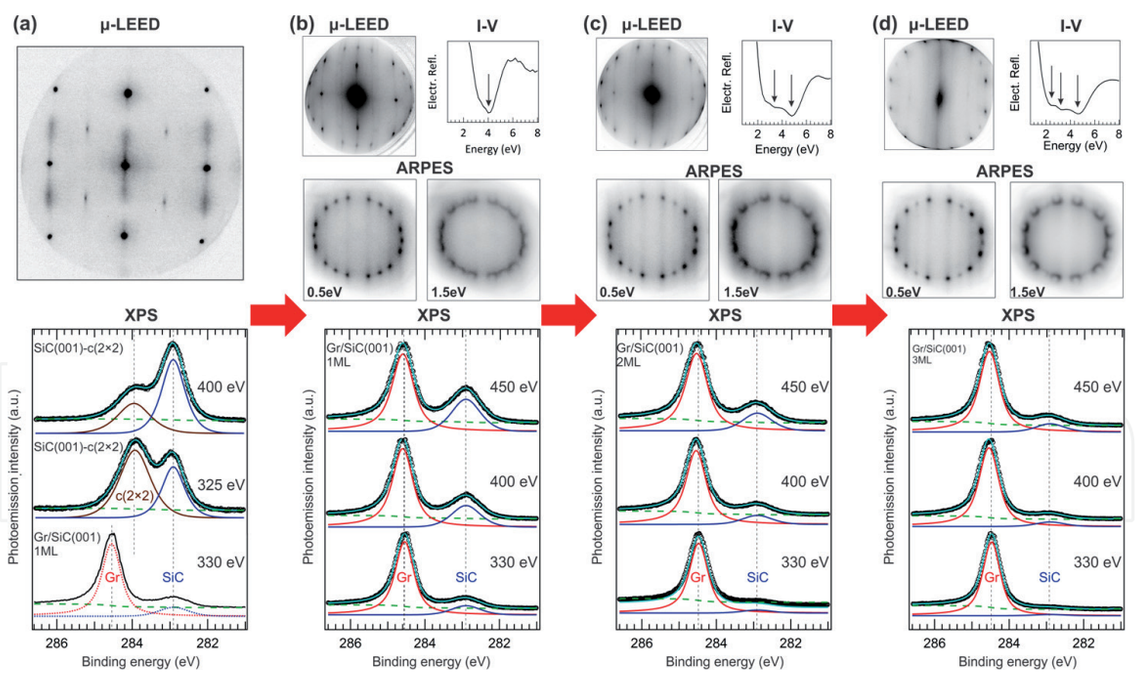

Figure 8.
In-situ LEEM, μ-LEED, ARPES, and XPS showing control over the SiC(001) surface graphitization during heating in UHV. (a) μ-LEED (top) and μ-XPS data (bottom) obtained from the SiC(001)-c(2 × 2) reconstruction. To illustrate the difference between the c(2 × 2) and graphene spectra, the C 1s spectrum from the 1 ML graphene/SiC(001) system is presented (bottom line). (b–d) μ-LEED, LEEM I-V reflectivity spectra, ARPES constant energy maps, and μ-XPS data obtained from one of APDs of the graphene/SiC(001) system at approximately 1 ML (b), 2 ML (c), and 3 ML (d) coverage. Top row: μ-LEED taken from a circular sample area (d = 0.5 μm) using a 44 eV electron beam (left) and LEEM I-V curves demonstrating one (b), two (c), and three (d) minima (indicated by arrows) corresponding to the number of the synthesized graphene layers (right). Middle row: Photoemission angular distribution maps taken at 0.5 eV (left) and 1.5 eV (right) binding energies, measured using a 47 eV photon energy. Bottom row: C 1s core level spectra (black circles) obtained with 330, 400 and 450 eV photon beams for 1, 2 and 3 ML from a circular sample areas (d = 2 μm) and results of the spectra decomposition. Reproduced from Ref. [102] with permission of ACS.

graphene peak (Gr), the blue line is the bulk SiC peak, the brown line is the surface β-SiC(001)-c(2 × 2) component, the green dashed line is the background and the cyan line is the envelope. One can note that each spectrum displays only two main components. The Gr peak is shifted by ~1.65 eV toward higher BE relative to the bulk SiC peak located at 282.9 eV. The intensity of the bulk SiC component decreases both with decreasing photon energy and increasing number of graphene layers. No other components except Gr and SiC were detected in the C 1s spectra, confirming the absence of strong chemical interactions between the graphene overlayer and β-SiC, which would provide additional components with higher BE [103]. The intensities of the individual components in the photoemission spectra shown in **Figure 8** can be used as a reference to distinguish between mono-, bi-, and trilayer graphene on the β-SiC/Si(001) wafers using XPS technique only. Measuring the XPS spectra in the normal emission geometry with 330, 400, and 450 eV photon energies, using the fast dynamic-XPS stations with real-time control of the core level spectra shape [109], one can stop the synthesis procedure when a desirable number of graphene layers (1, 2, or 3 ML) is synthesized.

The *in-situ* ARPES and μ-LEED measurements (**Figure 8**) uncover the origin of the 12 singular spots located between 12 double spots in the LEED pattern taken from the trilayer graphene synthesized on β-SiC(001) (**Figure 2(d)**) and explain the mechanism of the layer-by-layer graphene growth. The singular spots in **Figure 2(d)** are aligned with the SiC substrate spots in contrast with the ±13.5° rotated diffraction patterns corresponding to the rotated graphene nanodomain lattices shown in **Figure 3**. The middle row of images in **Figure 8** shows the ARPES intensity constant-energy maps taken at $E = E_F - 0.5$ eV and $E = E_F - 1.5$ eV as a function of graphene coverage. The ARPES maps prove the conical shape of the Fermi surface for all preferential graphene nanodomain lattice orientations (two non-rotated lattices and four lattices rotated by ±13.5° relative to the two orthogonal <110> directions) at three graphene coverages studied. Notably, both μ-LEED and ARPES maps measured for the 1 ML graphene/SiC(001) system reveal almost the same intensities of the features corresponding to the non-rotated and ± 13.5° rotated domain lattices. The intensity of the diffraction spots and ARPES features corresponding to the non-rotated lattices is systematically suppressed when graphene coverage increases from 1 ML (**Figure 8(b)**) to 2 ML (**Figure 8(c)**), and then to 3 ML (**Figure 8(d)**). The non-rotated graphene lattice orientations are prevailing only at the beginning of the β-SiC(001) surface graphitization. In contrast, when graphene coverage reaches several monolayers, most of the β-SiC(001) surface is covered by nanodomains with four preferential graphene lattice orientations, rotated ±13.5° relative to the two orthogonal <110> directions (**Figure 2(d)**).

Figure 9 shows **(a)** LEEM and **(b–e)** ARPES data obtained from the 1 ML graphene/β-SiC(001) sample. **Figure 9(b)** and **(c)** shows the constant energy ARPES intensity maps measured from different APDs marked as B and C on panel **(a)**. **Figure 9(d)** and **(e)** shows the dispersions obtained by a cut through the experimental data as indicated by the dashed lines in panels **(b)** and **(c)**, respectively. Eighteen identical linear dispersions are clearly resolved, proving that domains with all six preferential lattice orientations at 1 ML graphene coverage exhibit the same electronic structure typical of free-standing monolayer graphene.

The prevalence of the μ-LEED and ARPES features associated with the non-rotated lattices at sub-monolayer coverages is a key to understand the mechanism of the graphene growth on the β-SiC/Si(001) wafers. **Figure 10(a–c)** illustrates how the non-rotated graphene domain lattice can match the SiC(001)-c(2 × 2) reconstruction. If the lattice parameters of the c(2 × 2) square unit cell (red square) are doubled, it matches well to a slightly distorted square (green lines) connecting carbon atoms of the graphene lattice, which can be laterally translated to cover

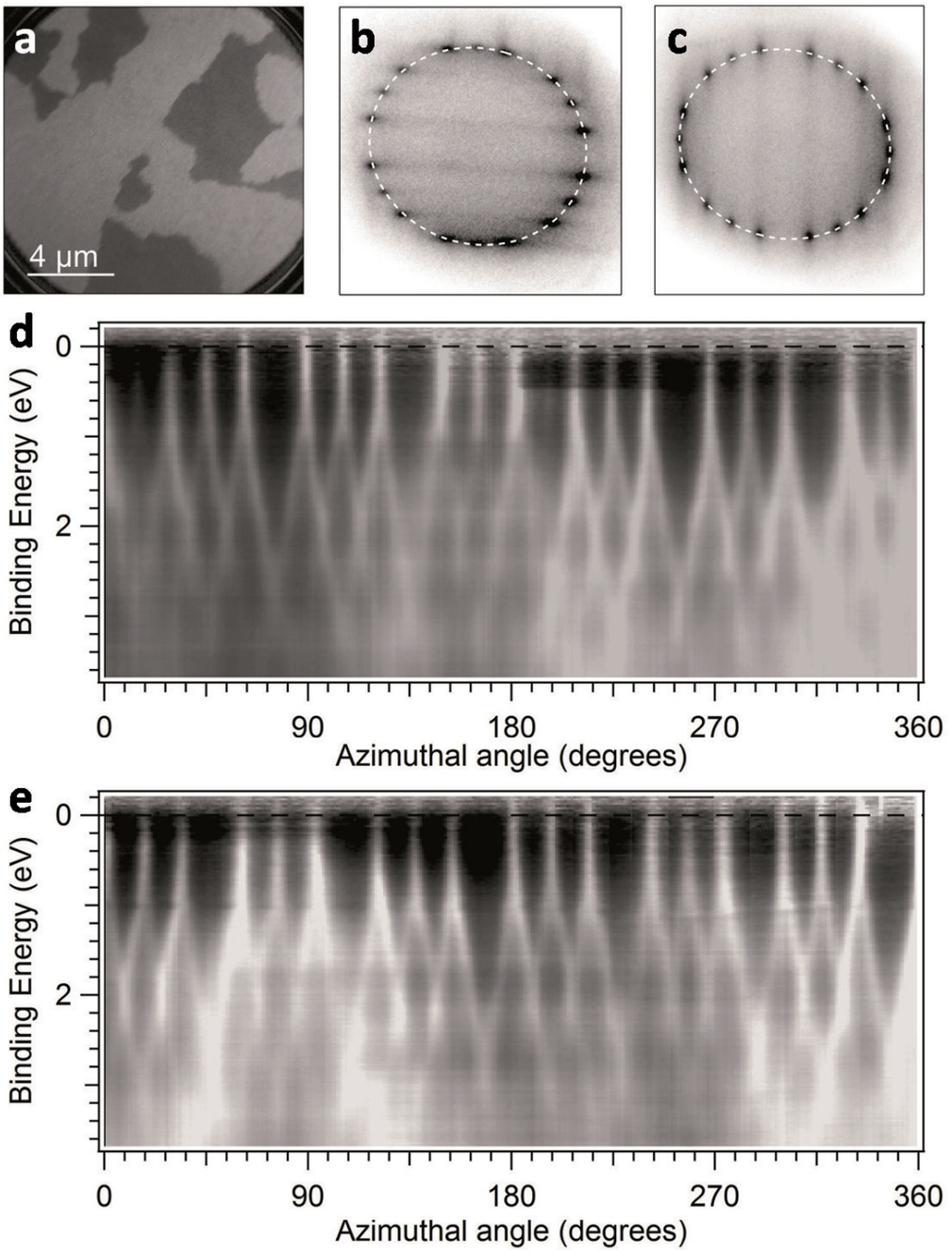

Figure 9.
LEEM and ARPES characterization of the nanostructured monolayer graphene. (a) DF-LEEM taken from the 1ML graphene/SiC(001) system. (b) and (c) Corresponding photoemission patterns taken for domains B and C in panel (a) at $E - E_F = 0.5$ eV, from a circular sample area (d = 2 μm, hν = 47 eV). (d) and (e) Dispersion of the Dirac cones obtained by a cut through the data as shown by the dashed lines in patterns (b) and (c). Reproduced from Ref. [102] with permission of ACS.

the entire c(2 × 2) surface by the graphene overlayer (**Figure 10(a)** and **(c)**). The mismatch of these two quadrilaterals is below 2%, which is likely sufficient to initiate the growth of the non-rotated graphene monolayer on SiC(001)-c(2 × 2). Such a small mismatch cannot be found for other possible surface structures. Therefore, the SiC(001)-c(2 × 2) reconstruction is a necessary step for successful high-temperature graphene synthesis on β-SiC(001). This is very similar to results of the STM studies performed on β-SiC(111) [71], where the transition from a typical $(\sqrt{3} \times \sqrt{3})$R30° to an intermediate $(3/2 \times \sqrt{3})$R30° structure matching the graphene (2 × 2) unit cell was observed before the formation of the honeycomb (1 × 1) overlayer.

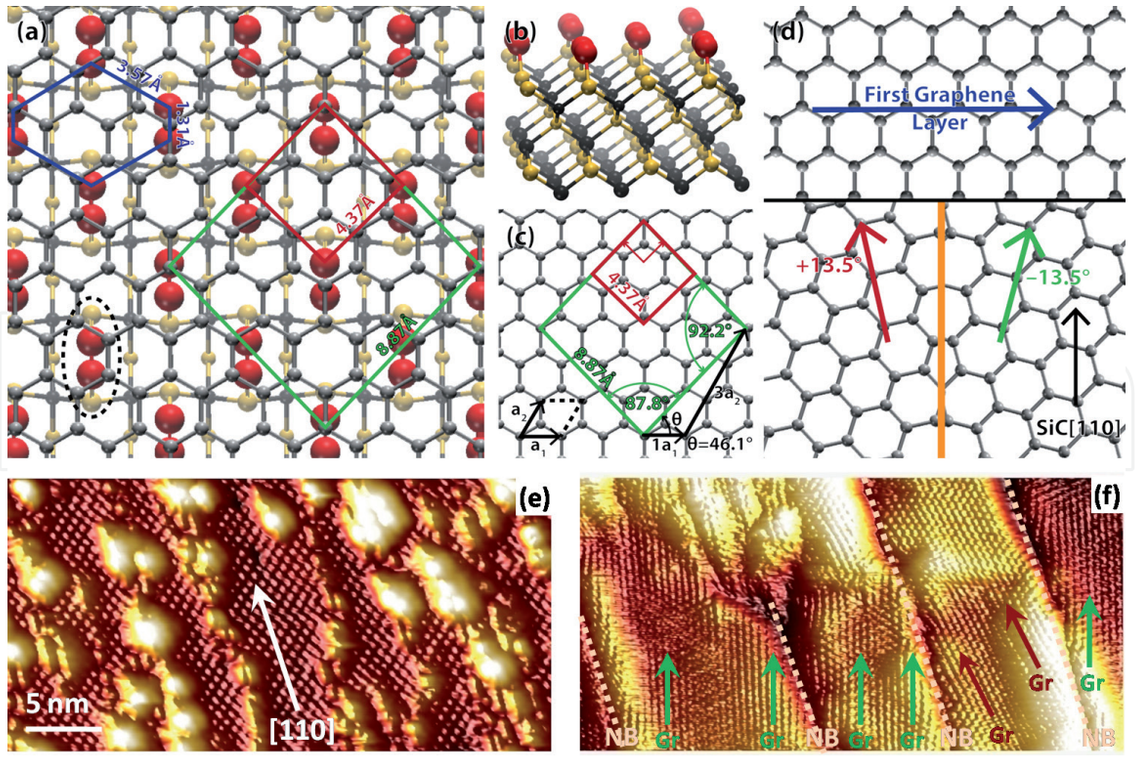

Figure 10.
Model of few-layer graphene growth on β-SiC(001). (a) A schematic model showing the non-rotated graphene lattice on top of the SiC(001)-c(2 × 2) reconstruction. Carbon and silicon atoms are shown as gray and yellow spheres, respectively, with c(2 × 2) carbon dimers highlighted by red spheres. The red square indicates the c(2 × 2) unit cell, the green square shows the distorted coincidence quadrilateral resembling a doubled c(2 × 2) unit cell. (b) Quasi-3D view of the SiC(001)-c(2 × 2) reconstruction. (c) A model of the graphene honeycomb lattice with the quadrilaterals showing the surface and overlayer cells. (d) A schematic model of the few-layer graphene growth on SiC(001): At the beginning, domains with a non-rotated honeycomb lattice nucleate in accordance with panel (a), then ±13.5°-rotated lattices start to grow from the linear defects, which become the nanodomain boundaries in the nanostructured graphene overlayer. (e,f) Atomically resolved STM images of the SiC(001)-c(2 × 2) surface (e) and trilayer graphene synthesized on a β-SiC/Si(001) wafer (f). Reproduced from Ref. [102] with permission of ACS.

The model in **Figure 10** suggests that carbon dimers of the c(2 × 2) reconstruction (indicated by dotted black oval in **Figure 10(a)**) may be considered the smallest building blocks of the non-rotated graphene lattice, since the distance between carbon atoms in the dimers (1.31 Å) is reasonably close to that of the graphene honeycomb lattice (1.46 Å). In order for graphene growth to begin, extra carbon atoms must be present on the c(2 × 2) surface to provide the substantially higher density of carbon atoms in the graphene lattice. Additional carbon atoms are actually observed during the STM studies as random bright protrusions (**Figure 1**) or linear <110>-directed atomic chains decorating the SiC(001)-c(2 × 2) reconstruction (**Figure 10(e)**). These adatoms form chemical bonds with the dimers of the c(2 × 2) reconstruction at high temperatures and initiate the preferential growth of graphene nanodomains with lattices non-rotated relative to the SiC <110> directions. These domains cannot grow to micrometer-scale due to the presence of linear defects on the SiC(001)-c(2 × 2) surface (**Figure 10(e)**) and the mismatch between the c(2 × 2) and graphene lattices producing strain in the overlayer. However, the reasonably small mismatch of the c(2 × 2) and the graphene lattice (**Figure 10(a)**) leads to the prevalence of the two non-rotated lattice variants in the graphene/SiC(001) system until the first monolayer is complete. The next layers presumably grow on top of the first monolayer starting from the linear defects on the surface (either steps or < 110>-directed linear atomic chains), which is supported by the very fast suppression of the non-rotated domain features in the μ-LEED and ARPES maps with increasing graphene coverage (**Figure 8**). The second and third graphene layers can

start to grow from the linear defects line-by-line [114] which define the positions and orientations of the nanodomain boundaries in the few-layer graphene/β-SiC(001) (**Figure 10(f)**). In this case, it is energetically favorable for graphene lattices in neighboring nanodomains to be rotated by 27° relative to one another, as the model in **Figure 10(d)** (bottom part) illustrates. The comparison of the atomic resolution STM images of the SiC(001)-c(2 × 2) and trilayer graphene/SiC(001) clearly shows the coincidence of the carbon atomic chain directions in the former structure (**Figure 10(e)**) and nanodomain boundary directions in the latter (**Figure 10(f)**). This result suggests that controlling the density and orientation of defects on β-SiC/Si(001) (e.g., steps on vicinal substrates) could allow the average size of the graphene domains and their orientation to be tuned. This can open a way for synthesis of self-aligned graphene nanoribbons supported by the technologically relevant β-SiC substrate.

4. Fabrication of self-aligned graphene nanoribbons using β-SiC thin films grown on vicinal Si(001) wafers

Synthesis of the uniform self-aligned trilayer graphene nanoribbon structure using β-SiC thin films grown on the vicinal Si(001) wafers with a miscut of 2° was reported in Ref. [93]. STM studies revealed that nanodomains on the vicinal sample are preferentially elongated in one direction (coinciding with the step direction of the bare SiC(001) substrate). This is illustrated in **Figure 11(a)** and **(b)**. Remarkably, the direction of the nanodomain boundaries in the trilayer graphene was the same in different APDs of the 2°-off β-SiC/Si(001) sample [93]. **Figure 11(c)** shows an atomically resolved STM image containing three nanodomains and three boundaries (NB). Detailed analysis of the STM images measured from various graphene/SiC/Si(001) samples showed that NBs are frequently rotated by 3.5° relative to the [110] crystallographic direction as depicted in **Figure 11(e)**. Since the graphene lattices in neighboring nanodomains are rotated by ±13.5° from the same [110] direction, they are asymmetrically rotated relative to the NBs. The lattices in neighboring domains are rotated by 10° counterclockwise (Gr_L)) and 17° clockwise (Gr_R) relative to the

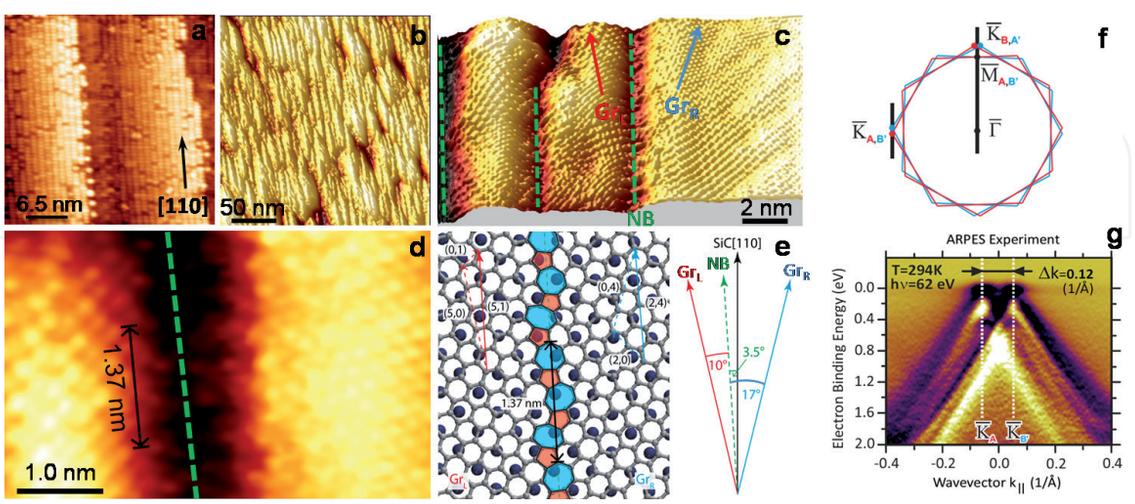

Figure 11.
(a) STM image of the vicinal SiC(001)-3 × 2 surface. The step direction is close to the [110] direction of the SiC crystal lattice. (b) Large-area STM image of graphene nanoribbons synthesized on the vicinal SiC(001). (c) and (d) Atomically resolved STM images of the graphene surface. The domain lattices are rotated 17° clockwise (Gr_R) and 10° anticlockwise (Gr_L) relative to the NB. The NB is itself rotated 3.5° anticlockwise from the [110] direction. (e) Schematic model of the NB for the asymmetrically rotated nanodomains in panels (c) and (d). For the angles shown a periodic structure of distorted pentagons and heptagons is formed. (f) Effective surface Brillouin zone corresponding to four rotated graphene domain variants. (g) Dispersion of the π-band in the graphene along the K_A-K_B direction indicated in panel (f) [93].

NB (**Figure 11(c)**). As **Figure 11(e)** illustrates, this asymmetry leads to the formation of a periodic structure along the boundaries, with a period of 1.37 nm. The periodic structure consists of distorted heptagons and pentagons, which is consistent with the atomically resolved STM image measured at the NB (**Figure 11(d)**). ARPES measurements, conducted on the same sample, showed sharp linear dispersions in the K-points for all preferential graphene lattice orientations (**Figure 11(f)** and **(g)**).

Recent theoretical studies [115] have demonstrated that graphene domain boundaries with a periodic atomic structure can reflect electrons over a large range of energies. This would provide a possibility to control the charge carriers in graphene without the need to introduce an energy bandgap. **Figure 12(a)** shows a schematic of a graphene nanogap device utilized for investigations of the transport properties of graphene synthesized on the β-SiC/2°-off Si(001) wafer [93]. The voltage was applied perpendicular to the nanodomain boundaries to investigate the local transport properties of the self-aligned nanoribbon system with asymmetrically rotated graphene domain lattices (**Figure 11**). According to the theory [115], a charge transport gap of $E_g = \hbar v_F \frac{2\pi}{3d} \approx \frac{1.38}{d(\text{nm})}$ (eV) could be induced by a non-symmetric rotation of graphene lattices in neighboring domains, where $\hbar$ is the reduced Planck's constant, v_F is the Fermi velocity, and d is the periodicity along the NB. As indicated in **Figure 11(d)** and **(e)**, the asymmetric rotation of the graphene lattices in the nanostructured trilayer graphene synthesized on β-SiC/2°-off Si(001) leads to a 1.37 nm periodicity along the NB. The formation of this periodic structure could be responsible for a transport gap of about 1.0 eV, which was observed in the low-temperature transport measurements (**Figure 12**). The transport gap is observed at temperatures below 100 K (**Figure 12(b)** and **(c)**). According to the *dI/dV* spectra shown in **Figure 12(d)**, the transport gap is ~1.3 eV at 50 and 10 K and substantially smaller (~0.4 eV) at 100 K. The conductivity of the trilayer graphene/β-SiC(001) nanogap device is only 0.01 μS at small voltages

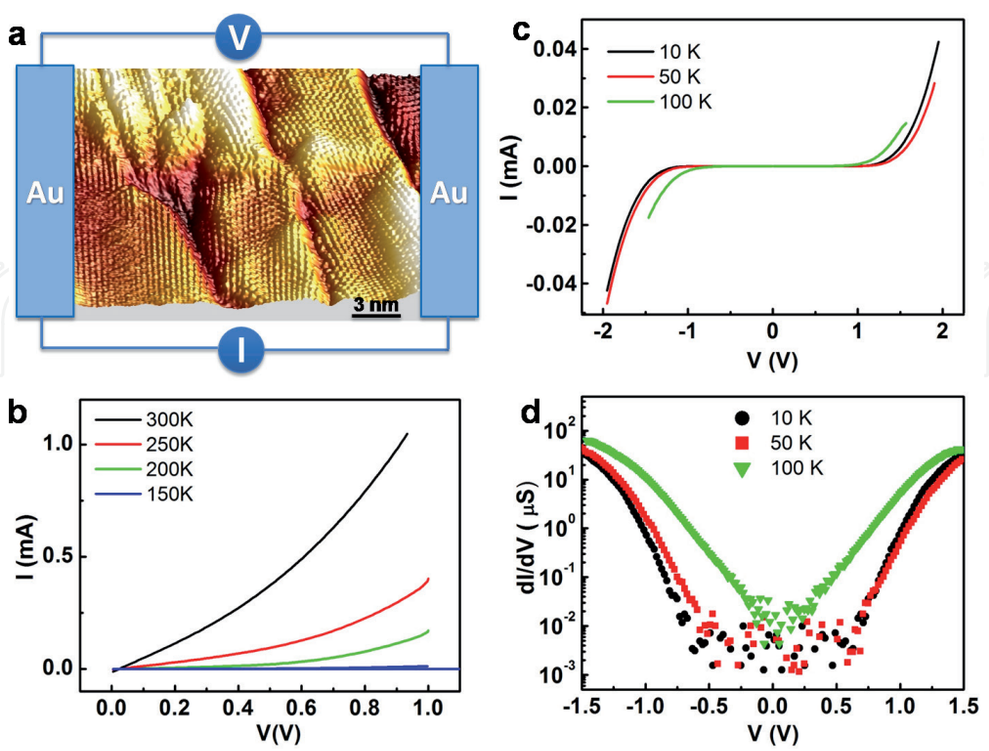

Figure 12.
(a) Schematic drawing of the nanogap device fabricated on the trilayer graphene/β-SiC/2°-off Si(001) sample. (b) I-V curves measured at 150, 200, 250 and 300 K. (c) I-V curves measured at 10, 50, and 100 K. (b) and (c) are measured with the current directed across the self-aligned NBs. (d) Corresponding dI/dV curves for temperatures below 150 K. Reproduced from Ref. [93] with permission of ACS.

and 100 μS at larger voltages when the electric current start to flow. This gives a high on-off current ratio of 10^4.

This successful demonstration of the transport gap opening in the nanostructured trilayer graphene (**Figure 12**) became possible because the NBs were uniformly aligned with the step direction of the vicinal β-SiC(001) substrate (**Figure 11**), i.e., perpendicular to the current direction in the electric measurements. Note that although the NBs with asymmetrical rotation of the graphene lattices were most frequently observed, boundaries with other atomic structures were also resolved in detailed atomic resolution STM studies of several few-layer graphene/β-SiC/Si(001) samples [85, 87, 93, 101, 102]. Despite the differences in the atomic structure, STM images generally revealed extreme distortions of the overlayer near the NBs (e.g., **Figures 1(g)** and **12**). The graphene overlayer in these areas was usually bent upward and downward, forming semi-tubes with typical diameters of several nanometers. According to the STM data, the radii of curvature of the ripples in the few-layer graphene on β-SiC/Si(001) wafers were typically in the range of 2–5 nm [101]. As revealed the theoretical calculations and recent experimental studies [101], the ripples formed at the NBs could also be responsible for the opening transport gap in graphene/β-SiC/Si(001). The self-aligned nanodomain boundaries with ripples can also be utilized to add the spin degree of freedom to graphene [101], since spin-orbit coupling can be induced by the curvature of the ripples [116].

5. Conclusions

We have summarized the results of high-resolution studies of the atomic and electronic structure of few-layer graphene synthesized in UHV on β-SiC thin films epitaxially grown on the technologically relevant Si(001) wafers. LEEM, μ-LEED, ARPES, and STM studies revealed that graphene overlayer on the β-SiC/Si(001) substrates consists of nanodomains with six preferential lattice orientations and two preferential nanodomain boundary directions. The number of the boundary directions can be reduced to one using vicinal wafers with small miscuts from the Si(001) plane. Thus, self-aligned graphene nanoribbon system supported by a wide-gap semiconductor substrate could be fabricated using 2°-off Si(001) wafer. *In-situ* studies of the few-layer graphene synthesis on the β-SiC/Si(001) wafers performed in UHV using micro-spectroscopic methods demonstrate that thickness of the graphene overlayer can be controlled in the course of the high-temperature synthesis and the procedure can be stopped when a desirable number of graphene layers (e.g., 1, 2, or 3 ML) is synthesized.

Acknowledgements

This work was carried out within the state task of ISSP RAS and supported by the Russian Foundation for Basic Research (Grant nos. 17-02-01139, 17-02-01291) and Erasmus plus mobility grant (2016-1-IE02-KA107-000479). We thank our colleagues S.V. Babenkov, H.-C. Wu, S.N. Molotkov, D. Marchenko, A. Varykhalov, A.A. Zakharov, B.E. Murphy, A. Locatelli, T.O. Menteş, S.L. Molodtsov, D.V. Potorochin, J. Buck, O. Seeck, M. Hoesch, and J. Viefhaus for fruitful discussions and help in the preparation of this manuscript.

Conflict of interest

The authors declare that there is no conflict of interest.

Author details

Olga V. Molodtsova[1], Alexander N. Chaika[2*] and Victor Yu. Aristov[1,2]

1 Deutsches Elektronen-Synchrotron DESY, Hamburg, Germany

2 Institute of Solid State Physics of the Russian Academy of Sciences, Russian Federation

*Address all correspondence to: chaika@issp.ac.ru

References

[1] Novoselov KS, Geim AK, Morozov SV, et al. Electric field effect in atomically thin carbon films. Science. 2004;**306**:666-669. DOI: 10.1126/science.1102896

[2] Geim AK, Novoselov KS. The rise of graphene. Nature Materials. 2007;**6**: 183-191. DOI: 10.1038/nmat1849

[3] Zhang Y, Tan Y-W, Stormer HL, Kim P. Experimental observation of the quantum Hall effect and Berry's phase in graphene. Nature. 2005;**438**:201-204. DOI: 10.1038/nature04235

[4] Novoselov KS, Geim AK, Morozov SV, et al. Two-dimensional gas of massless Dirac fermions in graphene. Nature. 2005;**438**:197-200. DOI: 10.1038/nature04233

[5] Han W, Kawakami RK, Gmitra M, Fabian J. Graphene spintronics. Nature Nanotechnology. 2014;**9**:794-807. DOI: 10.1038/nnano.2014.214

[6] Yang T-Y, Balakrishnan J, Volmer F, et al. Observation of long spin-relaxation times in bilayer graphene at room temperature. Physical Review Letters. 2011;**107**:047206. DOI: 10.1103/PhysRevLett.107.047206

[7] Dlubak B, Martin M-B, Deranlot C, et al. Highly efficient spin transport in epitaxial graphene on SiC. Nature Physics. 2012;**8**:557-561. DOI: 10.1038/nphys2331

[8] Novoselov KS. Nobel lecture: Graphene: Materials in the Flatland. Reviews of Modern Physics. 2011;**83**:837-849. DOI: 10.1103/RevModPhys.83.837

[9] Novoselov KS, Fal′ko VI, Colombo L, Gellert PR, Schwab MG, Kim K. A roadmap for graphene. Nature. 2012;**490**:192-200. DOI: 10.1038/nature11458

[10] Chen Z, Lin Y-M, Rooks MJ, Avouris P. Graphene nano-ribbon electronics. Physica E (Low-dimensional Systems and Nanostructures). 2007;**40**:228-232. DOI: 10.1016/j.physe.2007.06.020

[11] de Heer WA, Berger C, Wu X, et al. Epitaxial graphene. Solid State Communications. 2007;**143**:92-100. DOI: 10.1016/j.ssc.2007.04.023

[12] Geim AK. Graphene: Status and prospects. Science. 2009;**324**:1530-1534. DOI: 10.1126/science.1158877

[13] Berger C. Electronic confinement and coherence in patterned epitaxial graphene. Science. 2006;**312**:1191-1196. DOI: 10.1126/science.1125925

[14] Hernandez Y, Nicolosi V, Lotya M, et al. High-yield production of graphene by liquid-phase exfoliation of graphite. Nature Nanotechnology. 2008;**3**: 563-568. DOI: 10.1038/nnano.2008.215

[15] Bolotin KI, Sikes KJ, Jiang Z, et al. Ultrahigh electron mobility in suspended graphene. Solid State Communications. 2008;**146**:351-355. DOI: 10.1016/j.ssc.2008.02.024

[16] Du X, Skachko I, Barker A, Andrei EY. Approaching ballistic transport in suspended graphene. Nature Nanotechnology. 2008;**3**:491-495. DOI: 10.1038/nnano.2008.199

[17] Jiao L, Zhang L, Wang X, Diankov G, Dai H. Narrow graphene nanoribbons from carbon nanotubes. Nature. 2009;**458**:877-880. DOI: 10.1038/nature07919

[18] Choucair M, Thordarson P, Stride JA. Gram-scale production of graphene based on solvothermal synthesis and sonication. Nature Nanotechnology. 2009;**4**:30-33. DOI: 10.1038/nnano.2008.365

[19] Chakrabarti A, Lu J, Skrabutenas JC, et al. Conversion of carbon dioxide to few-layer graphene. Journal of Materials Chemistry. 2011;**21**:9491. DOI: 10.1039/c1jm11227a

[20] Rümmeli MH, Gorantla S, Bachmatiuk A, et al. On the role of vapor trapping for chemical vapor deposition (CVD) grown graphene over copper. Chemistry of Materials. 2013;**25**:4861-4866. DOI: 10.1021/cm401669k

[21] Li X, Cai W, An J, et al. Large-area synthesis of high-quality and uniform graphene films on copper foils. Science. 2009;**324**:1312-1314. DOI: 10.1126/science.1171245

[22] Rümmeli MH, Bachmatiuk A, Scott A, et al. Direct low-temperature nanographene CVD synthesis over a dielectric insulator. ACS Nano. 2010;**4**:4206-4210. DOI: 10.1021/nn100971s

[23] Wei D, Xu X. Laser direct growth of graphene on silicon substrate. Applied Physics Letters. 2012;**100**:023110. DOI: 10.1063/1.3675636

[24] Michon A, Tiberj A, Vézian S, et al. Graphene growth on AlN templates on silicon using propane-hydrogen chemical vapor deposition. Applied Physics Letters. 2014;**104**:071912. DOI: 10.1063/1.4866285

[25] Chen J, Wen Y, Guo Y, et al. Oxygen-aided synthesis of polycrystalline graphene on silicon dioxide substrates. Journal of the American Chemical Society. 2011;**133**:17548-17551. DOI: 10.1021/ja2063633

[26] Wang G, Zhang M, Zhu Y, et al. Direct growth of graphene film on germanium substrate. Scientific Reports. 2013;**3**:2465. DOI: 10.1038/srep02465

[27] Tang S, Ding G, Xie X, et al. Nucleation and growth of single crystal graphene on hexagonal boron nitride. Carbon N Y. 2012;**50**:329-331. DOI: 10.1016/j.carbon.2011.07.062

[28] Hwang J, Kim M, Campbell D, et al. van der Waals epitaxial growth of graphene on sapphire by chemical vapor deposition without a metal catalyst. ACS Nano. 2013;**7**:385-395. DOI: 10.1021/nn305486x

[29] Ismach A, Druzgalski C, Penwell S, et al. Direct chemical vapor deposition of graphene on dielectric surfaces. Nano Letters. 2010;**10**:1542-1548. DOI: 10.1021/nl9037714

[30] Pasternak I, Wesolowski M, Jozwik I, et al. Graphene growth on Ge(100)/Si(100) substrates by CVD method. Scientific Reports. 2016;**6**:21773. DOI: 10.1038/srep21773

[31] Van Bommel AJ, Crombeen JE, Van Tooren A. LEED and Auger electron observations of the SiC(0001) surface. Surface Science. 1975;**48**:463-472. DOI: 10.1016/0039-6028(75)90419-7

[32] Forbeaux I, Themlin J-M, Debever J-M. Heteroepitaxial graphite on 6H-SiC(0001): Interface formation through conduction-band electronic structure. Physical Review B. 1998;**58**:16396-16406. DOI: 10.1103/PhysRevB.58.16396

[33] Virojanadara C, Syväjarvi M, Yakimova R, Johansson LI, Zakharov AA, Balasubramanian T. Homogeneous large-area graphene layer growth on 6H-SiC(0001). Physical Review B. 2008;**78**:245403. DOI: 10.1103/PhysRevB.78.245403

[34] Emtsev KV, Bostwick A, Horn K, et al. Towards wafer-size graphene layers by atmospheric pressure graphitization of silicon carbide. Nature Materials. 2009;**8**:203-207. DOI: 10.1038/nmat2382

[35] Ohta T, Bostwick A, Seyller T, Horn K, Rotenberg E. Controlling the

electronic structure of bilayer graphene. Science. 2006;**313**:951-954. DOI: 10.1126/science.1130681

[36] Riedl C, Starke U, Bernhardt J, Franke M, Heinz K. Structural properties of the graphene-SiC(0001) interface as a key for the preparation of homogeneous large-terrace graphene surfaces. Physical Review B. 2007;**76**:245406. DOI: 10.1103/PhysRevB.76.245406

[37] First PN, de Heer WA, Seyller T, Berger C, Stroscio JA, Moon J-S. Epitaxial graphenes on silicon carbide. MRS Bulletin. 2010;**35**:296-305. DOI: 10.1557/mrs2010.552

[38] Berger C, Song Z, Li T, et al. Ultrathin epitaxial graphite: 2D electron gas properties and a route toward graphene-based nanoelectronics. The Journal of Physical Chemistry. B. 2004;**108**:19912-19916. DOI: 10.1021/jp040650f

[39] Hass J, de Heer WA, Conrad EH. The growth and morphology of epitaxial multilayer graphene. Journal of Physics. Condensed Matter. 2008;**20**:323202. DOI: 10.1088/0953-8984/20/32/323202

[40] de Heer WA, Berger C, Wu X, et al. Epitaxial graphene electronic structure and transport. Journal of Physics D: Applied Physics. 2010;**43**:374007. DOI: 10.1088/0022-3727/43/37/374007

[41] Tejeda A, Taleb-Ibrahimi A, de Heer W, Berger C, Conrad EH. Electronic structure of epitaxial graphene grown on the C-face of SiC and its relation to the structure. New Journal of Physics. 2012;**14**:125007. DOI: 10.1088/1367-2630/14/12/125007

[42] Sprinkle M, Siegel D, Hu Y, et al. First direct observation of a nearly ideal graphene band structure. Physical Review Letters. 2009;**103**:226803. DOI: 10.1103/PhysRevLett.103.226803

[43] Nishino S, Powell JA, Will HA. Production of large-area single-crystal wafers of cubic SiC for semiconductor devices. Applied Physics Letters. 1983;**42**:460-462. DOI: 10.1063/1.93970

[44] Feng ZC, Mascarenhas AJ, Choyke WJ, Powell JA. Raman scattering studies of chemical-vapor-deposited cubic SiC films of (100) Si. Journal of Applied Physics. 1988;**64**:3176-3186. DOI: 10.1063/1.341533

[45] Shigeta M, Fujii Y, Furukawa K, Suzuki A, Nakajima S. Chemical vapor deposition of single-crystal films of cubic SiC on patterned Si substrates. Applied Physics Letters. 1989;**55**: 1522-1524. DOI: 10.1063/1.102252

[46] Golecki I, Reidinger F, Marti J. Single-crystalline, epitaxial cubic SiC films grown on (100) Si at 750°C by chemical vapor deposition. Applied Physics Letters. 1992;**60**:1703-1705. DOI: 10.1063/1.107191

[47] Coletti C, Frewin CL, Saddow SE, Hetzel M, Virojanadara C, Starke U. Surface studies of hydrogen etched 3C-SiC(001) on Si(001). Applied Physics Letters. 2007;**91**:061914. DOI: 10.1063/1.2768870

[48] Miyamoto Y, Handa H, Saito E, et al. Raman-scattering spectroscopy of epitaxial graphene formed on SiC film on Si substrate. e-Journal of Surface Science and Nanotechnology. 2009;**7**: 107-109. DOI: 10.1380/ejssnt.2009.107

[49] Suemitsu M, Miyamoto Y, Handa H, Konno A. Graphene formation on a 3C-SiC(111) thin film grown on Si(110) substrate. e-Journal of Surface Science and Nanotechnology. 2009;**7**: 311-313. DOI: 10.1380/ejssnt.2009.311

[50] Aristov VY, Urbanik G, Kummer K, et al. Graphene synthesis on cubic SiC/Si wafers. Perspectives for mass production of graphene-based

electronic devices. Nano Letters. 2010;**10**:992-995. DOI: 10.1021/nl904115h

[51] Suemitsu M, Fukidome H. Epitaxial graphene on silicon substrates. Journal of Physics D: Applied Physics. 2010;**43**:374012. DOI: 10.1088/0022-3727/43/37/374012

[52] Fukidome H, Miyamoto Y, Handa H, Saito E, Suemitsu M. Epitaxial growth processes of graphene on silicon substrates. Japanese Journal of Applied Physics. 2010;**49**:01AH03. DOI: 10.1143/JJAP.49.01AH03

[53] Ouerghi A, Kahouli A, Lucot D, et al. Epitaxial graphene on cubic SiC(111)/Si(111) substrate. Applied Physics Letters. 2010;**96**:191910. DOI: 10.1063/1.3427406

[54] Ouerghi A, Belkhou R, Marangolo M, et al. Structural coherency of epitaxial graphene on 3C–SiC(111) epilayers on Si(111). Applied Physics Letters. 2010;**97**:161905. DOI: 10.1063/1.3497287

[55] Abe S, Handa H, Takahashi R, Imaizumi K, Fukidome H, Suemitsu M. Surface chemistry involved in epitaxy of graphene on 3C-SiC(111)/Si(111). Nanoscale Research Letters. 2010;**5**:1888-1891. DOI: 10.1007/s11671-010-9731-x

[56] Ouerghi A, Marangolo M, Belkhou R, et al. Epitaxial graphene on 3C-SiC(111) pseudosubstrate: Structural and electronic properties. Physical Review B. 2010;**82**:125445. DOI: 10.1103/PhysRevB.82.125445

[57] Coletti C, Emtsev KV, Zakharov AA, Ouisse T, Chaussende D, Starke U. Large area quasi-free standing monolayer graphene on 3C-SiC(111). Applied Physics Letters. 2011;**99**:081904. DOI: 10.1063/1.3618674

[58] Takahashi R, Handa H, Abe S, et al. Low-energy-electron-diffraction and X-ray-photoelectron-spectroscopy studies of graphitization of 3C-SiC(111) thin film on Si(111) substrate. Japanese Journal of Applied Physics. 2011;**50**:070103. DOI: 10.1143/JJAP.50.070103

[59] Handa H, Takahashi R, Abe S, et al. Transmission electron microscopy and Raman-scattering spectroscopy observation on the interface structure of graphene formed on Si substrates with various orientations. Japanese Journal of Applied Physics. 2011;**50**:04DH02. DOI: 10.1143/JJAP.50.04DH02

[60] Otsuji T, Boubanga Tombet SA, Satou A, et al. Graphene-based devices in terahertz science and technology. Journal of Physics D: Applied Physics. 2012;**45**:303001. DOI: 10.1088/0022-3727/45/30/303001

[61] Portail M, Michon A, Vézian S, et al. Growth mode and electric properties of graphene and graphitic phase grown by argon–propane assisted CVD on 3C–SiC/Si and 6H–SiC. Journal of Crystal Growth. 2012;**349**:27-35. DOI: 10.1016/j.jcrysgro.2012.04.004

[62] Starke U, Coletti C, Emtsev K, Zakharov AA, Ouisse T, Chaussende D. Large area quasi-free standing monolayer graphene on 3C-SiC(111). Materials Science Forum. 2012; **717-720**:617-620. DOI: 10.4028/www.scientific.net/MSF.717-720.617

[63] Coletti C, Forti S, Principi A, et al. Revealing the electronic band structure of trilayer graphene on SiC: An angle-resolved photoemission study. Physical Review B. 2013;**88**:155439. DOI: 10.1103/PhysRevB.88.155439

[64] Darakchieva V, Boosalis A, Zakharov AA, et al. Large-area microfocal spectroscopic ellipsometry mapping of thickness and electronic properties of epitaxial graphene on Si- and C-face of 3C-SiC(111). Applied

Physics Letters. 2013;**102**:213116. DOI: 10.1063/1.4808379

[65] Aryal HR, Fujita K, Banno K, Egawa T. Epitaxial graphene on Si(111) substrate grown by annealing 3C-SiC/carbonized silicon. Japanese Journal of Applied Physics. 2012;**51**:01AH05. DOI: 10.1143/JJAP.51.01AH05

[66] Fukidome H, Abe S, Takahashi R, et al. Controls over structural and electronic properties of epitaxial graphene on silicon using surface termination of 3C-SiC(111)/Si. Applied Physics Express. 2011;**4**:115104. DOI: 10.1143/APEX.4.115104

[67] Sanbonsuge S, Abe S, Handa H, et al. Improvement in film quality of epitaxial graphene on SiC(111)/Si(111) by SiH_4 pretreatment. Japanese Journal of Applied Physics. 2012;**51**:06FD10. DOI: 10.1143/JJAP.51.06FD10

[68] Hsia B, Ferralis N, Senesky DG, Pisano AP, Carraro C, Maboudian R. Epitaxial graphene growth on 3C–SiC(111)/AlN(0001)/Si(100). Electrochemical and Solid-State Letters. 2011;**14**:K13. DOI: 10.1149/1.3518713

[69] Jiao S, Murakami Y, Nagasawa H, et al. High quality graphene formation on 3C-SiC/4H-AlN/Si heterostructure. Materials Science Forum. 2014;**806**: 89-93. DOI: 10.4028/www.scientific.net/MSF.806.89

[70] Gupta B, Notarianni M, Mishra N, Shafiei M, Iacopi F, Motta N. Evolution of epitaxial graphene layers on 3C SiC/Si (111) as a function of annealing temperature in UHV. Carbon N Y. 2014;**68**:563-572. DOI: 10.1016/j.carbon.2013.11.035

[71] Gupta B, Placidi E, Hogan C, Mishra N, Iacopi F, Motta N. The transition from 3C SiC(111) to graphene captured by Ultra High Vacuum Scanning Tunneling Microscopy. Carbon N Y. 2015;**91**:378-385. DOI: 10.1016/j.carbon.2015.05.011

[72] Pierucci D, Sediri H, Hajlaoui M, et al. Evidence for flat bands near the fermi level in epitaxial rhombohedral multilayer graphene. ACS Nano. 2015;**9**:5432-5439. DOI: 10.1021/acsnano.5b01239

[73] Zarotti F, Gupta B, Iacopi F, Sgarlata A, Tomellini M, Motta N. Time evolution of graphene growth on SiC as a function of annealing temperature. Carbon N Y. 2016;**98**:307-312. DOI: 10.1016/j.carbon.2015.11.026

[74] Gupta B, Di Bernardo I, Mondelli P, et al. Effect of substrate polishing on the growth of graphene on 3C-SiC(111)/Si(111) by high temperature annealing. Nanotechnology. 2016;**27**:185601. DOI: 10.1088/0957-4484/27/18/185601

[75] Shi Y, Zakharov AA, Ivanov IG, et al. Elimination of step bunching in the growth of large-area monolayer and multilayer graphene on off-axis 3C-SiC (111). Carbon N Y. 2016;**140**:533-542. DOI: 10.1016/j.carbon.2018.08.042

[76] Bouhafs C, Stanishev V, Zakharov AA, et al. Decoupling and ordering of multilayer graphene on C-face 3C-SiC(111). Applied Physics Letters. 2016;**109**:203102. DOI: 10.1063/1.4967525

[77] Sambonsuge S, Jiao S, Nagasawa H, et al. Formation of qualified epitaxial graphene on Si substrates using two-step heteroexpitaxy of C-terminated 3C-SiC(-1-1-1) on Si(110). Diamond and Related Materials. 2016;**67**:51-53. DOI: 10.1016/j.diamond.2016.02.020

[78] Nemec L, Lazarevic F, Rinke P, et al. Why graphene growth is very different on the C face than on the Si face of SiC: Insights from surface equilibria and the (3×3)-3C-SiC(-1-1-1) reconstruction. Physical Review B. 2015;**91**:161408. DOI: 10.1103/PhysRevB.91.161408

[79] Mondelli P, Gupta B, Betti MG, et al. High quality epitaxial graphene by hydrogen-etching of 3C-SiC(111) thin-film on Si(111). Nanotechnology. 2017;**28**:115601. DOI: 10.1088/1361-6528/aa5a48

[80] Amjadipour M, MacLeod J, Lipton-Duffin J, et al. Epitaxial graphene growth on FIB patterned 3C-SiC nanostructures on Si (111): Reducing milling damage. Nanotechnology. 2017;**28**:345602. DOI: 10.1088/1361-6528/aa752e

[81] Amjadipour M, Tadich A, Boeckl JJ, et al. Quasi free-standing epitaxial graphene fabrication on 3C-SiC/Si(111). Nanotechnology. 2018;**29**:145601. DOI: 10.1088/1361-6528/aaab1a

[82] Ouerghi A, Ridene M, Balan A, et al. Sharp interface in epitaxial graphene layers on 3C-SiC(100)/Si(100) wafers. Physical Review B. 2011;**83**:205429. DOI: 10.1103/PhysRevB.83.205429

[83] Gogneau N, Balan A, Ridene M, Shukla A, Ouerghi A. Control of the degree of surface graphitization on 3C-SiC(100)/Si(100). Surface Science. 2012;**606**:217-220. DOI: 10.1016/j.susc.2011.09.021

[84] Ouerghi A, Balan A, Castelli C, et al. Epitaxial graphene on single domain 3C-SiC(100) thin films grown on off-axis Si(100). Applied Physics Letters. 2012;**101**:021603. DOI: 10.1063/1.4734396

[85] Chaika AN, Molodtsova OV, Zakharov AA, et al. Continuous wafer-scale graphene on cubic-SiC(001). Nano Research. 2013;**6**:562-570. DOI: 10.1007/s12274-013-0331-9

[86] Abe S, Handa H, Takahashi R, Imaizumi K, Fukidome H, Suemitsu M. Temperature-programmed desorption observation of graphene-on-silicon process. Japanese Journal of Applied Physics. 2011;**50**:070102. DOI: 10.1143/JJAP.50.070102

[87] Chaika AN, Molodtsova OV, Zakharov AA, et al. Rotated domain network in graphene on cubic-SiC(001). Nanotechnology. 2014;**25**:135605. DOI: 10.1088/0957-4484/25/13/135605

[88] Velez-Fort E, Silly MG, Belkhou R, Shukla A, Sirotti F, Ouerghi A. Edge state in epitaxial nanographene on 3C-SiC(100)/Si(100) substrate. Applied Physics Letters. 2013;**103**:083101. DOI: 10.1063/1.4818547

[89] Gogneau N, Ben Gouider Trabelsi A, et al. Investigation of structural and electronic properties of epitaxial graphene on 3C-SiC(100)/Si(100) substrates. Nanotechnology, Science and Applications. 2014;**7**:85. DOI: 10.2147/NSA.S60324

[90] Hens P, Zakharov AA, Iakimov T, Syväjärvi M, Yakimova R. Large area buffer-free graphene on non-polar (001) cubic silicon carbide. Carbon N Y. 2014;**80**:823-829. DOI: 10.1016/j.carbon.2014.09.041

[91] Suemitsu M, Jiao S, Fukidome H, Tateno Y, Makabe I, Nakabayashi T. Epitaxial graphene formation on 3C-SiC/Si thin films. Journal of Physics D: Applied Physics. 2014;**47**:094016. DOI: 10.1088/0022-3727/47/9/094016

[92] Iacopi F, Mishra N, Cunning BV, et al. A catalytic alloy approach for graphene on epitaxial SiC on silicon wafers. Journal of Materials Research. 2015;**30**:609-616. DOI: 10.1557/jmr.2015.3

[93] Wu H-C, Chaika AN, Huang T-W, et al. Transport gap opening and high on-off current ratio in trilayer graphene with self-aligned nanodomain boundaries. ACS Nano. 2015;**9**:8967-8975. DOI: 10.1021/acsnano.5b02877

[94] Huang H, Liang Wong S, Tin C-C, et al. Epitaxial growth and characterization of graphene on free-standing polycrystalline 3C-SiC. Journal

of Applied Physics. 2011;**110**:014308. DOI: 10.1063/1.3602993

[95] Ide T, Kawai Y, Handa H, et al. Epitaxy of graphene on 3C-SiC(111) thin films on microfabricated Si(111) substrates. Japanese Journal of Applied Physics. 2012;**51**:06FD02. DOI: 10.1143/JJAP.51.06FD02

[96] Cunning BV, Ahmed M, Mishra N, Kermany AR, Wood B, Iacopi F. Graphitized silicon carbide microbeams: Wafer-level, self-aligned graphene on silicon wafers. Nanotechnology. 2014;**25**:325301. DOI: 10.1088/0957-4484/25/32/325301

[97] Fukidome H, Kawai Y, Fromm F, et al. Precise control of epitaxy of graphene by microfabricating SiC substrate. Applied Physics Letters. 2012;**101**:041605. DOI: 10.1063/1.4740271

[98] Bantaculo R, Fukidome H, Suemitsu M. Correlation between the residual stress in 3C-SiC/Si epifilm and the quality of epitaxial graphene formed thereon. IOP Conference Series Materials Science and Engineering. 2015;**79**:012004. DOI: 10.1088/1757-899X/79/1/012004

[99] Yazdi GR, Vasiliauskas R, Iakimov T, Zakharov A, Syväjärvi M, Yakimova R. Growth of large area monolayer graphene on 3C-SiC and a comparison with other SiC polytypes. Carbon N Y. 2013;**57**:477-484. DOI: 10.1016/j.carbon.2013.02.022

[100] Fukidome H, Ide T, Kawai Y, et al. Microscopically-tuned band structure of epitaxial graphene through interface and stacking variations using Si substrate microfabrication. Scientific Reports. 2015;**4**:5173. DOI: 10.1038/srep05173

[101] Wu H-C, Chaika AN, Hsu M-C, et al. Large positive in-plane magnetoresistance induced by localized states at nanodomain boundaries in graphene. Nature Communications. 2017;**8**:14453. DOI: 10.1038/ncomms14453

[102] Aristov VY, Chaika AN, Molodtsova OV, et al. Layer-by-layer graphene growth on β-SiC/Si(001). ACS Nano. 2019;**13**:526-535. DOI: 10.1021/acsnano.8b07237

[103] Chaika AN, Aristov VY, Molodtsova OV. Graphene on cubic-SiC. Progress in Materials Science. 2017;**89**:1-30. DOI: 10.1016/j.pmatsci.2017.04.010

[104] Fasolino A, Los JH, Katsnelson MI. Intrinsic ripples in graphene. Nature Materials. 2007;**6**:858-861. DOI: 10.1038/nmat2011

[105] Meyer JC, Geim AK, Katsnelson MI, Novoselov KS, Booth TJ, Roth S. The structure of suspended graphene sheets. Nature. 2007;**446**:60-63. DOI: 10.1038/nature05545

[106] Hibino H, Kageshima H, Maeda F, Nagase M, Kobayashi Y, Yamaguchi H. Microscopic thickness determination of thin graphite films formed on SiC from quantized oscillation in reflectivity of low-energy electrons. Physical Review B. 2008;**77**:075413. DOI: 10.1103/PhysRevB.77.075413

[107] Riedl C, Coletti C, Iwasaki T, Zakharov AA, Starke U. Quasi-free-standing epitaxial graphene on SiC obtained by hydrogen intercalation. Physical Review Letters. 2009;**103**:246804. DOI: 10.1103/PhysRevLett.103.246804

[108] Shirley EL, Terminello LJ, Santoni A, Himpsel FJ. Brillouin-zone-selection effects in graphite photoelectron angular distributions. Physical Review B. 1995;**51**:13614-13622. DOI: 10.1103/PhysRevB.51.13614

[109] Babenkov SV, Aristov VY, Molodtsova OV, et al. A new

dynamic-XPS end-station for beamline PO_4 at PETRA III/DESY. Nuclear Instruments and Methods in Physics Research Section A: Accelerators, Spectrometers, Detectors and Associated Equipment. 2015;**777**:189-193. DOI: 10.1016/j.nima.2014.12.065

[110] Aristov VY. β-SiC(100) surface: Atomic structures and electronic properties. Physics-Uspekhi. 2001;**44**:761-783. DOI: 10.1070/PU2001v044n08ABEH000979

[111] Soukiassian PG, Enriquez HB. Atomic scale control and understanding of cubic silicon carbide surface reconstructions, nanostructures and nanochemistry. Journal of Physics. Condensed Matter. 2004;**16**:S1611-S1658. DOI: 10.1088/0953-8984/16/17/011

[112] Hupalo M, Conrad EH, Tringides MC. Growth mechanism for epitaxial graphene on vicinal 6 H-SiC(0001) surfaces: A scanning tunneling microscopy study. Physical Review B. 2009;**80**:041401. DOI: 10.1103/PhysRevB.80.041401

[113] Wang Q, Zhang W, Wang L, He K, Ma X, Xue Q. Large-scale uniform bilayer graphene prepared by vacuum graphitization of 6H-SiC(0001) substrates. Journal of Physics. Condensed Matter. 2013;**25**:095002. DOI: 10.1088/0953-8984/25/9/095002

[114] Patera LL, Bianchini F, Africh C, et al. Real-time imaging of adatom-promoted graphene growth on nickel. Science. 2018;**359**:1243-1246. DOI: 10.1126/science.aan8782

[115] Yazyev OV, Louie SG. Electronic transport in polycrystalline graphene. Nature Materials. 2010;**9**:806-809. DOI: 10.1038/nmat2830

[116] Huertas-Hernando D, Guinea F, Brataas A. Spin-orbit coupling in curved graphene, fullerenes, nanotubes, and nanotube caps. Physical Review B. 2006;**74**:155426. DOI: 10.1103/PhysRevB.74.155426